Physica Scripta

INCLUSIVE PUBLISHING
TRUSTED SCIENCE

PAPER

Modelling and simulation of electrical analogous for permanent magnet materials

To cite this article: Antonio Paulo Rodrigues Fernandez *et al* 2023 *Phys. Scr.* **98** 115025

View the article online for updates and enhancements.

You may also like

- Laser-induced ultrafast transport and demagnetization at the earliest time: first-principles and real-time investigation
G P Zhang, Y H Bai, Tyler Jenkins et al.
- Evidence for Asteroid Scattering and Distal Solar System Solids From Meteorite Paleomagnetism
James F. J. Bryson, Benjamin P. Weiss, Eduardo A. Lima et al.
- Micromagnetics of rare-earth efficient permanent magnets
Johann Fischbacher, Alexander Kovacs, Markus Gusenbauer et al.

This content was downloaded from IP address 143.107.255.190 on 16/11/2023 at 12:51

Physica Scripta

PAPER

Modelling and simulation of electrical analogous for permanent magnet materials

RECEIVED
7 June 2023

REVISED
14 August 2023

ACCEPTED FOR PUBLICATION
5 October 2023

PUBLISHED
17 October 2023

Antonio Paulo Rodrigues Fernandez[1], **Elio Alberto Perigo**[2] and **Rubens Nunes de Faria Junior**[1,*]

[1] Nuclear and Energy Research Institute, Sao Paulo, 05508-000, Brazil
[2] ABB Corporate Research Center, Raleigh, NC 27606, United States of America
[*] Author to whom any correspondence should be addressed.

E-mail: aprfff@alumni.usp.br, eaperigo@ieee.org and rfaria@ipen.br

Keywords: permanent magnet mathematical modeling, RLC circuits, magnetization curve simulation, demagnetization curve simulation

Abstract

Expressions to simulate the intrinsic demagnetizing curve of permanent magnets are derived from the classical electrical analogy of a 2*RLC* circuit as an equivalent to a magnet under demagnetization in a closed magnetic circuit. Comparisons between experimental and theoretical intrinsic M x H curves were carried out for hard magnetic materials, and the possibility of using this analogous circuit with two components has also been investigated. The demagnetization curves of permanent sintered magnets have been simulated with time domain analytical expressions obtained using an electric equivalent circuit analogous to a closed magnetic circuit. This has been carried out for magnets measured at room temperature and at 373 K. Equivalent electric parameters influenced the various regions of the demagnetization curve. It has also been shown that it was possible to simulate the demagnetization curve of rare earth magnets and also other types of permanent magnets. The Stoner-Wohlfarth model theoretical curves have also been used as a comparison. At last, the electrical analogous parameters have been systematically varied in order to correlate them to the magnetic properties.

Symbol list:

Magnetic:

B_r	remanence; unit: tesla (T);
${}_iH_c$	intrinsic coercivity; unit: tesla (T);
${}_bH_c$	inductive coercivity; unit: tesla (T);
M_r	remanent polarization; unit: tesla (T);
M_s	saturation polarization; unit: tesla (T);
$\langle\cos\theta\rangle$	degree of crystal alignment;
f	volume fraction of the magnetic hard phase;
P	packing factor of the magnet;
PM	permanent magnet;
R_p	internal reluctance;
R_p^{-1}	internal permeance;

Electric:

C	fixed capacitance of the capacitor; unit: farad (F);
$i_1(t)$	intensity of the current present in the capacitor; unit: ampere (A);
$i_2(t)$	intensity of the current present in the resistor R_2; unit: ampere (A);
$i_3(t)$	intensity of the current present in the capacitor C; unit: ampere (A);

© 2023 IOP Publishing Ltd

j	the same as $\sqrt{-1}$;
L	input inductance of the inductor; unit: henry (H);
R_1	equivalent series resistance; unit: ohm (Ω);
R_2	equivalent parallel resistance; unit: ohm (Ω);
t	time elapsed in the processes of first charge, discharge and second charge of the capacitor C; unit: second (s);
$t_{(i1°PC)}$	time in which the first charging process of the capacitor C contained in the circuit $2RLC$ starts; unit: second (s);
$t_{(f1°PC)}$	time at which the end of the first charging process occurs; unit: second (s);
$t_{(iPD)}$	time in which the discharge of capacitor C contained in electrical circuit $2RLC$ starts; unit: second (s);
$t_{(fPD)}$	time in which the discharge of capacitor C in circuit $2RLC$ is completed; unit: second (s);
$t_{(i2°PC)}$	time in which the second charging process of capacitor C begins; unit: second (s);
$t_{(SC)}$	duration of a half-cycle of charge or discharge of capacitor C in circuit $2RLC$ of capacitor C contained in electrical circuit $2RLC$; unit: second (s);
$\Delta v(t)$	electric potential difference between the source of electromotive force terminals; unit: volt (V);
$\Delta v_C(t)$	electric potential difference between the capacitor C terminals; unit: volt (V);
$\Delta v_L(t)$	electric potential difference between the inductor L terminals; unit: volt (V);
x_1	the same as $-\left(\frac{R_1R_2C+L}{2R_2LC}-\sqrt{\left(\frac{R_1R_2C+L}{2R_2LC}\right)^2-\frac{R_1+R_2}{2R_2LC}}\right)$; unit: time inverse ($s^{-1}$);
x_2	the same as $-\left(\frac{R_1R_2C+L}{2R_2LC}+\sqrt{\left(\frac{R_1R_2C+L}{2R_2LC}\right)^2-\frac{R_1+R_2}{2R_2LC}}\right)$; unit: time inverse ($s^{-1}$);
x	the same as $\frac{R_1R_2C+L}{2R_2LC}$; unit: time inverse (s^{-1});
y	the same as $j\sqrt{\left(\frac{R_1R_2C+L}{2R_2LC}\right)^2-\frac{R_1+R_2}{R_2LC}}$, being that $\frac{R_1+R_2}{R_2LC}$ has units in inverse time squared (s^{-2});
z	the same as $\frac{R_1R_2C+L}{R_1+R_2}$; unit: time (s);
$\varepsilon(t)$	triangular electrical potential source;
β	rate of change of the electric potential as a function of time of the permeameter; unit: volts per second (Vs^{-1}).

1. Introduction

In the past, electrical analogous have been reported for viscoelastic systems [1, 2]. More recently, electrical analogous have been reported for an atomic force microscope and biomaterials [3, 4]. The purpose of the latter was to develop analog electrical circuits, using resistors, capacitors and constant current sources which automatically calculated the stress and strain-rate response of viscoelastic biomaterials. Furthermore, the *RLC* circuit has been reported as an analogy with mechanical systems [5]. The circuit was shown and its responses in the time domain in addition to a comparison between an electrical circuit and a mass-spring-damper. Moreover, the solution of partial differential equations by electrical analogy has been reported in the literature [6].

As far as permanent magnets analogies is concerned, the mechanical and electrostatic analogy to magnets has been reviewed for the purposes of developing an intuitive feel for the fashion in which energy is stored in a magnet and showed that it is useful to use analogies to other types of physical consideration [7]. The magnetic circuit representation of a magnet driving an external reluctance has been reviewed and the capacitive and mechanical analogies to a magnet were considered. It has been also shown that these analogies have an equivalent circuit representation that is identical to the one used to describe a magnet [7]. No extensive reports on the electrical analogy for permanent magnets have been published in the literature.

Typically, a sintered rare earth magnet has the characteristic intrinsic demagnetization curve M x H with two distinct regions [8]. Region 1 is the linear reversible part and region 2 corresponds to nonlinear irreversible behavior where partial undesirable demagnetization occurs at some locations in the magnet structure. The remanence (B_r) of a magnet is the highest polarization ($B_r = \mu_0 M_r$) obtained on a close magnetic circuit after saturation in a high pulsed magnetic field and this is the starting point of region one. If the polarization (M_r)

remains absolutely constant the magnet material permeability would be a horizontal line ($\mu_r = 1$). However, the permeability for the demagnetization curve of practical rare earth magnets is in the range of 1.04 to 1.10 [9]. This means, that some phases in addition to the hard magnet phase can exist in the magnets and has also been attributed to spin fluctuations or small nuclei of domains [9, 10]. The intrinsic coercivity defines the field where the polarization is reduced to zero [8]. This mostly vertical curve in region two of the intrinsic curve is characterized by the presence of demagnetizing fields (N) in the grain structure of real magnets and the slope of this deviation from the vertical line is given by N^{-1} [11].

The intrinsic curve of an ideal magnet would be composed by just two lines forming a rectangular shape and a unitary squareness factor (SF) [12]. The larger the squareness factor the closer the magnetic permeability is to unity and the stronger the capacity of the material to resist a demagnetizing field. It also has a better stability to temperature variations and a very small inclination of the horizontal line. The squareness factor is sensitive to the material purity and alloy composition, processing conditions, grain size, homogeneity, rare earth and oxygen content, abnormal or irregular grains. A mathematical equation to simulate the intrinsic curve of a magnet must provide means to modify the horizontal slope of the linear reversible part of the curve and also the vertical linear part of the intrinsic curve. Furthermore, in the nonlinear irreversible region this equation must provide a smooth connection between these two lines accordingly to the squareness factor and the knee field (H_k) [12, 13].

The classical approach in modeling magnetic circuits uses the electric circuit analogy of Ohm's Law [14–17]. In this case, the normal (or inductive) demagnetization curve B x H is the relevant data for applications including motors and generators. For these purposes, a permanent magnet (PM) can be represented by a Thevenin equivalent circuit composed by a magnetomotive force source in series with an internal reluctance (R_p) or by a Norton equivalent circuit composed by a flux source in parallel with an internal permeance (R_p^{-1}). Similarities and dissimilarities can be found in this analogy [18]. Concerning the former, equivalent circuits use resistances to represent magnetic reluctances and voltage sources to represent magneto-motive forces. Regarding the differences, an example is the contradiction in modeling magnetic cores that store energy with dissipative components such as resistances which impairs the energy and power equivalence [19]. To overcome this particular objection, a magnetic capacitor has been introduced in the equivalent electric equivalent circuits [20].

For the modeling of the intrinsic demagnetization curve M x H, which represents the response of the highly complex material of a PM, the described approach used for the inductive demagnetization curve B x H with a flux source in parallel with a permeance is unsatisfactory and a more complex configuration must be evaluated. It has recently been demonstrated the possibility to simulate curves of electrochemical capacitors using a straightforward electrical circuit [21]. The aim of this study is to solve the problem of simulating the intrinsic demagnetization curve of permanent magnets using the classical analogy between magnetic and electric circuits. The starting point was to deduce the ODE for a circuit containing the three principal electric components. Thus, the present study proposes analytical equations governing a theoretical analogous electric circuit for a PM using a capacitor, an inductor, two resistances and a direct current source. Comparisons between experimental and theoretical intrinsic M x H demagnetization curves were carried out for permanent magnets, and the possibility of using this analogous circuit with only two components has also been investigated. At last, the electrical analogous parameters have been systematically varied in order to correlate them to the magnetic properties.

The organizational structure of this article has been divided into four parts. Firstly, deduction of the equations through which it is possible to simulate magnetic hysteresis loops by means of the solution of ordinary differential equations (ODE) obtained from the analysis in the time domain of an electrical RLC circuit fed by a triangular electromotive force source. Secondly, proof of the functionality of the deduced equations by comparing the yielded theoretical loops with the Stoner-Wohlfarth model, also based on a theoretical model [22]. Thirdly, the functionality of the equations deduced in this study is compared to demagnetization curves of real permanent magnets. Finally, various possible electric circuit configurations to simulate magnetic curves are also discussed and, at last, conclusions are presented.

2. Equivalent circuits and equations

Here the second quadrant curve M x H of a PM is modeled using an equivalence between a magnet contained in a closed magnetic circuit with an electrical analogy circuit depicted in figure 1. The simulation is based on the intensity of the electric current $i_1(t)$ present in the terminals of an electric circuit 2RLC fed by a source of triangular electric potential $\varepsilon(t)$. It must be noted that the shape of the demagnetization curve is highly sensitive to the magnetizing field and saturation must be ensured (and considered in the next sections) for the PM.

The expressions that make it possible to calculate the intensity of $i_1(t)$ existent at the electric circuit will be presented for three conditions, namely:

- First charge process up to a maximum positive potential;

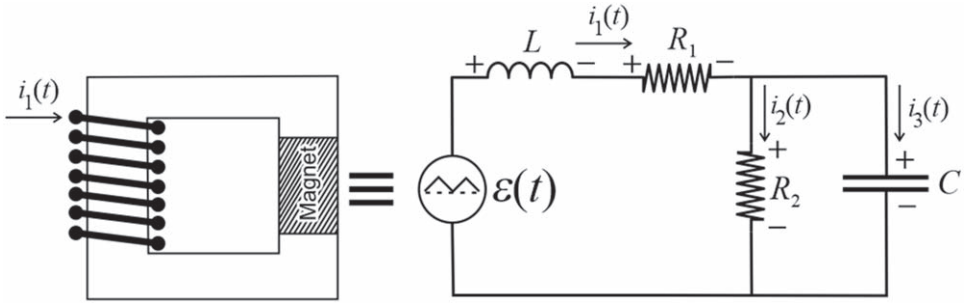

Figure 1. Charging process of the capacitor C contained in the electrical circuit $2RLC$ powered by a triangular electric potential source $\varepsilon(t)$, which is assumed to be analogous or equivalent to a permanent magnet in a closed demagnetization circuit.

- First discharge process from the maximum positive potential up to a maximum negative potential of the same magnitude as the maximum positive potential; and
- Discharge process from the maximum negative potential to the maximum positive potential. In this last cycle of discharge and charge of the capacitor C contained in the circuit $2RLC$, the equation is obtained that allows to calculate the values of $i_1(t)$ used to simulate the second quadrant of a permanent magnet.

Figure 1 also illustrates schematically the current directions in the first charging process of the capacitor C contained in the electrical circuit $2RLC$ powered by a triangular potential source $\varepsilon(t)$. For the first charging process of the capacitor C, it is verified that:

$$\varepsilon(t) = \Delta v_L(t) + i_1(t)R_1 + \Delta v_C(t), \tag{1}$$

where $\Delta v_L(t)$ is the electric potential between the terminals of the inductor L and $\Delta v_C(t)$ is the electrical potential between the terminals of the capacitor C.

The potential of the triangular electrical potential source, represented by ε(t) in the previous equation, is dictated by:

$$\varepsilon(t) = (-1)^n \beta[2(n-1)\, t_{(SC)} - t], \tag{2}$$

where n represents the number of variations that the source presents between a maximum positive value and a maximum negative value (or *vice versa*) of electric potential (or between a null value and a maximum positive or maximum negative value of electric potential), and β indicates the rate of change of the potential difference between the terminals of the triangular electromotive force source as a function of time. Therefore, for example, if the $2RLC$ electrical circuit needs to be charged by a maximum instantaneous potential difference, $\Delta v(t)$, that varies between $+1$ V and -1 V and, considering that it is initially discharged and the source starts from a potential voltage of 0 V (which is common in order to avoid load short circuit) until it reaches a value of $+1$ V, then $n = 1$. After the terminals of the $2RLC$ circuit present a potential of $+1$ V to source, the discharge and charge operations proceed with negative electrical potential until the terminals of the $2RLC$ circuit present a value of -1 V, $n = 2$. When $n = 3$, the source starts the operation of discharging and charging with positive electrical potential until the terminals of the $2RLC$ circuit present a value of $+1$ V, and so on.

2.1. Charging process equivalent to the magnetization process

Based on the analysis of the $2RLC$ circuit shown in figure 1 and on the expression of the triangular source signal shown in equation (2) for n equal to 1, equation (3) was obtained. Through this equation it is possible to calculate the instantaneous intensity of the current $i_1(t)$ present in the branch of the source for the first process of charging the capacitor. It should be noted that several steps to obtain equation (3) were omitted, as well as the possible expressions for the second-order ODE solutions originating from the analysis of the circuit presented in figure 1 for the capacitor charging process. Equation (3) was derived for the condition in which $[(R_1R_2C + L)/2R_2LC]^2 - (R_1 + R_2)/R_2LC > 0$ (see equation (6) e (7) as follow).

$$i_1(t) = A_1 e^{x_1 t}\left(\frac{1}{R_2} + Cx_1\right) + A_2 e^{x_2 t}\left(\frac{1}{R_2} + Cx_2\right) + \frac{\beta}{R_1 + R_2}(t + R_2C - z), \tag{3}$$

Equation (3) allows to calculate the values of $i_1(t)$ for the first charge process of the capacitor C in the electric circuit $2RLC$, fed by a triangular electric potential source, $\varepsilon(t)$, considering the ODE solution of second linear and non-homogeneous order.

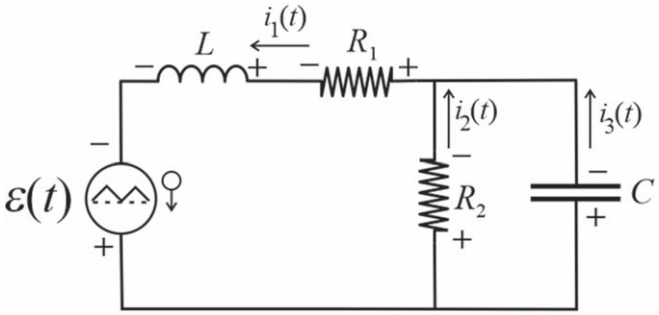

Figure 2. Discharge process of the capacitor C contained in the electrical circuit $2RLC$ governed by a triangular electric potential source $\varepsilon(t)$.

In equation (3) we have that:

$$A_1 = -\frac{\beta R_2}{(x_1 - x_2)(R_1 + R_2)}(1 + x_2 z); \tag{4}$$

$$A_2 = \frac{\beta R_2}{(x_1 - x_2)(R_1 + R_2)}(1 + x_1 z); \tag{5}$$

$$x_1 = -\left(\frac{R_1 R_2 C + L}{2R_2 LC} - \sqrt{\left(\frac{R_1 R_2 C + L}{2R_2 LC}\right)^2 - \frac{R_1 + R_2}{2R_2 LC}}\right); \tag{6}$$

$$x_2 = -\left(\frac{R_1 R_2 C + L}{2R_2 LC} + \sqrt{\left(\frac{R_1 R_2 C + L}{2R_2 LC}\right)^2 - \frac{R_1 + R_2}{2R_2 LC}}\right); \tag{7}$$

$$z = \frac{R_1 R_2 C + L}{R_1 + R_2}. \tag{8}$$

2.2. Discharging process of capacitor C equivalent to reducing the magnetization field to zero

In order to obtain the expression the allows the calculation the values of $i_1(t)$ for the first discharge process and second reverse charg process of the capacitor C in the electrical circuit $2RLC$ governed by a triangular source $\varepsilon(t)$, the circuit presented in figure 2 was taken as a reference.

By means of equation (9) it is possible to calculate the intensity of the electric current $i_1(t)$ for the condition in which the first discharge process and the first reverse charge process of the capacitor C occurs in a 2RLC circuit due to annulment, gradual reduction and inversion of the existing potential difference between the terminals of the triangular electromotive force source, which is equivalent to saying that in equation (2) n became equal to 1.

$$i_1(t) = A_3 e^{x_1 t}\left(Cx_1 + \frac{1}{R_2}\right) + A_4 e^{x_2 t}\left(Cx_2 + \frac{1}{R_2}\right) + \frac{\beta}{R_1 + R_2}(2\, t_{(SC)} + z - t - R_2 C). \tag{9}$$

In the equation (9) we have that:

$$A_3 = A_1 + \frac{2\beta R_2 x_2}{e^{x_1 t_{(i1\circ PD)}}(x_1 - x_2)(R_1 + R_2)}\left(\frac{1}{x_2} - t_{(i1\circ PD)} + t_{(SC)} + z\right). \tag{10}$$

$$A_4 = A_2 - \frac{2\beta R_2 x_1}{e^{x_2 t_{(i1\circ PD)}}(x_1 - x_2)(R_1 + R_2)}\left(\frac{1}{x_1} - t_{(i1\circ PD)} + t_{(SC)} + z\right). \tag{11}$$

2.3. Second charging process equivalent to the demagnetization

By means of equation (12) it is possible to calculate the intensity of the electric current $i_1(t)$ for the condition in which the first process of reversed discharge and second process of charging of the capacitor occurs due to cancellation, gradual reduction and inversion of the potential difference existing between the terminals of the triangular source of electromotive force, which is equivalent to saying that in equation (2) n became equal to 2.

$$i_1(t) = A_5 e^{x_1 t}\left(\frac{1}{R_2} + Cx_1\right) + A_6 e^{x_2 t}\left(\frac{1}{R_2} + Cx_2\right) + \frac{\beta}{R_1 + R_2}(t + R_2 C - 4\, t_{(SC)} - z). \tag{12}$$

In equation (12) we have that:

$$A_5 = A_3 - \frac{2\beta R_2 x_2}{e^{x_1 t_{(i2\circ PC)}}(x_1 - x_2)(R_1 + R_2)}\left(\frac{1}{x_2} + 3\, t_{(SC)} + z - t_{(i2\circ PC)}\right), \tag{13}$$

$$A_6 = A_4 + \frac{2\beta R_2 x_1}{e^{x_2 t_{(i2\circ PC)}}(x_1 - x_2)(R_1 + R_2)}\left(\frac{1}{x_1} + 3\, t_{(SC)} + z - t_{(i2\circ PC)}\right). \tag{14}$$

The following equations were employed for $[(R_1R_2C + L)/2R_2LC]^2 - (R_1 + R_2)/R_2LC < 0$, they were used to plot the curves in figure 8 for the condition in which the terms contained in equations (6) and (7) started to result in negative values (the condition called 'negative root')

Making use of equation (15), shown below, it is possible to calculate the values of $i_1(t)$ for the first charge process of the capacitor C contained in the electric circuit $2RLC$, fed by a triangular electric potential source, $\varepsilon(t)$, by the condition $[(R_1R_2C + L)/2R_2LC]^2 - (R_1 + R_2)/R_2LC < 0$.

$$i_1(t) = \left\{\begin{array}{l} e^{-xt}\left\{\left[\frac{1}{R_2}A_7 - C(xA_8 - yA_7)\right]\cos(ty) + \left[\frac{1}{R_2}A_8 - C(yA_7 + xA_8)\right]\sin(ty)\right\} + \\ + \frac{\beta}{R_1 + R_2}(t - z + R_2C) \end{array}\right\}. \tag{15}$$

In equation (15) we have that:

$$A_7 = \frac{\beta R_2}{R_1 + R_2}z, \tag{16}$$

$$A_8 = \frac{\beta R_2(xz - 1)}{y(R_1 + R_2)}, \tag{17}$$

and

$$\frac{R_1R_2C + L}{2R_2LC} = x. \tag{18}$$

By means of the equation (19), presented below, it is possible to calculate the values of $i_1(t)$ for the first discharge process and the first reverse charge process of the capacitor C contained in the circuit $2RLC$ fed by a triangular electric potential source, $\varepsilon(t)$, by the condition $[(R_1R_2C + L)/2R_2LC]^2 - (R_1 + R_2)/R_2LC < 0$.

$$i_1(t) = \left\{\begin{array}{l} e^{-xt}\left\{\left[\frac{1}{R_2}A_9 - C(xA_{10} - yA_9)\right]\cos(ty) + \left[\frac{1}{R_2}A_{10} - C(yA_9 + xA_{10})\right]\sin(ty)\right\} \\ + \frac{\beta}{R_1 + R_2}(2\, t_{(SC)} + z - t - R_2C) \end{array}\right\} \tag{19}$$

In equation (19) we have that:

$$A_9 = \frac{\left\{\begin{array}{l} (y\cos(yt_{(i1\circ PD)}) - x\sin(yt_{(i1\circ PD)}))\left[\begin{array}{l} A_7\cos(yt_{(i1\circ PD)}) + A_8\sin(yt_{(i1\circ PD)}) + \\ + e^{xt_{(i1\circ PD)}}\frac{2\beta R_2}{R_1 + R_2}(t_{(i1\circ PD)} - z - t_{(SC)}) \end{array}\right] + \\ - \sin(yt_{(i1\circ PD)})\left[\begin{array}{l} (xA_8 - yA_7)\cos(yt_{(i1\circ PD)}) - (yA_7 + xA_8)\sin(yt_{(i1\circ PD)}) + \\ + e^{xt_{(i1\circ PD)}}\frac{2\beta R_2}{R_1 + R_2} \end{array}\right] \end{array}\right\}}{\sin(yt_{(i1\circ PD)})(y\sin(yt_{(i1\circ PD)}) + x\cos(yt_{(i1\circ PD)})) + \cos(yt_{(i1\circ PD)})(y\cos(yt_{(i1\circ PD)}) - x\sin(yt_{(i1\circ PD)}))}, \tag{20}$$

and

$$A_{10} = \frac{\left\{\begin{array}{l} (y\sin(yt_{(i1\circ PD)}) + x\cos(yt_{(i1\circ PD)}))\left[\begin{array}{l} A_7\cos(yt_{(i1\circ PD)}) + A_8\sin(yt_{(i1\circ PD)}) + \\ + e^{xt_{(i1\circ PD)}}\frac{2\beta R_2}{R_1 + R_2}(t_{(i1\circ PD)} - z - t_{(SC)}) \end{array}\right] + \\ + \cos(yt_{(i1\circ PD)})\left[\begin{array}{l} (xA_8 - yA_7)\cos(yt_{(i1\circ PD)}) - (yA_7 + xA_8)\sin(yt_{(i1\circ PD)}) + \\ + e^{xt_{(i1\circ PD)}}\frac{2\beta R_2}{R_1 + R_2} \end{array}\right] \end{array}\right\}}{\sin(yt_{(i1\circ PD)})(y\sin(yt_{(i1\circ PD)}) + x\cos(yt_{(i1\circ PD)})) + \cos(yt_{(i1\circ PD)})(y\cos(yt_{(i1\circ PD)}) - x\sin(yt_{(i1\circ PD)}))} \tag{21}$$

Using equation (22), disposed below, it is possible to calculate the values of $i_1(t)$ for the first reverse discharge process and second process charge of the capacitor C contained in the circuit $2RLC$ fed by a triangular electric potential source, $\varepsilon(t)$, by the condition $[(R_1R_2C + L)/2R_2LC]^2 - (R_1 + R_2)/R_2LC < 0$.

$$i_1(t) = \begin{Bmatrix} e^{-xt}\left\{\left[\frac{1}{R_2}A_{11} + C(yA_{12} - xA_{11})\right]\cos(ty) + \left[\frac{1}{R_2}A_{12} - C(yA_{11} + xA_{12})\right]\sin(ty)\right\} + \\ + \frac{\beta}{R_1 + R_2}(t + R_2C - 4\,t_{(SC)} - z) \end{Bmatrix} \quad (22)$$

In equation (22) we have that:

$$A_{11} = \frac{\begin{Bmatrix} (y\cos(yt_{(i2oPC)}) - x\sin(yt_{(i2oPC)}))\left[\begin{matrix} A_9\cos(yt_{(i2oPC)}) + A_{10}\sin(yt_{(i2oPC)}) + \\ + e^{xt_{(i2oPC)}}\frac{2\beta R_2}{R_1 + R_2}(3\,t_{(SC)} + z - t_{(i2oPC)}) \end{matrix}\right] \\ -\sin(yt_{(i2oPC)})\left[\begin{matrix} (yA_{10} - xA_9)\cos(yt_{(i2oPC)}) - (yA_9 + xA_{10})\sin(yt_{(i2oPC)}) + \\ + e^{xt_{(i2oPC)}}\frac{2\beta R_2}{R_1 + R_2} \end{matrix}\right] \end{Bmatrix}}{\cos(yt_{(i2oPC)})(y\cos(yt_{(i2oPC)}) - x\sin(yt_{(i2oPC)})) + \sin(yt_{(i2oPC)})(x\cos(yt_{(i2oPC)}) + y\sin(yt_{(i2oPC)}))} \quad (23)$$

and

$$A_{12} = \frac{\begin{Bmatrix} (x\cos(yt_{(i2oPC)}) + y\sin(yt_{(i2oPC)}))\left[\begin{matrix} A_9\cos(yt_{(i2oPC)}) + A_{10}\sin(yt_{(i2oPC)}) + \\ + e^{xt_{(i2oPC)}}\frac{2\beta R_2}{R_1 + R_2}(3\,t_{(SC)} + z - t_{(i2oPC)}) \end{matrix}\right] + \\ +\cos(yt_{(i2oPC)})\left[\begin{matrix} (yA_{10} - xA_9)\cos(yt_{(i2oPC)}) - (yA_9 + xA_{10})\sin(yt_{(i2oPC)}) + \\ - e^{xt_{(i2oPC)}}\frac{2\beta R_2}{R_1 + R_2} \end{matrix}\right] \end{Bmatrix}}{\sin(yt_{(i2oPC)})(x\cos(yt_{(i2oPC)}) + y\sin(yt_{(i2oPC)})) + \cos(yt_{(i2oPC)})(y\cos(yt_{(i2oPC)}) - x\sin(yt_{(i2oPC)}))}. \quad (24)$$

3. Experimental

The modeling proposed does not require any feature of the permanent magnet to be known, so that its implementation is material agnostic. In order to assess its results, the most common type of hard magnets rare-earth-based were explored to clarify correlations between (micro)structural characteristics, analogous electric parameters, and magnetic properties. For the case of rare-earth PMs, $Pr_{16}Fe_{76}B_8$ sintered permanent magnets with optimized processing conditions according to [23, 24] were used. The hysteresis shape quantification was determined using H_k/H_{cj} definition [12, 13]. Equivalent electric parameters used to yield modeled demagnetization curves were acquired via best fitting. It must be mentioned that the shape of the demagnetization curve is highly sensitive to the magnetizing field and saturation must be ensured for the rare earth permanent magnets. Although some vibrating sample magnetometers are capable of saturating the rare earth magnet, generally, this demagnetization curve is determined using a close circuit hysteresis-meter after magnet saturation in a high intensity magnetic field generated by capacitive pulse discharge on a magnetizing coil. The present model and equations only simulate curves of permanent magnets that have been fully magnetized to saturation. Distortions on the second quadrant demagnetization curves of rare earth magnets caused by poor magnetization have not been incorporated on the present model. Electrical units were omitted for the magnetic parameter and simulations since inside a real permanent magnet the electrical parameters are only imaginary figures.

4. Results and discussion

4.1. Stoner-wohlfarth loops

The classical theoretical loops yielded by mathematical expressions are presented in figure 3 (see 22). The data used yielded these theoretical curves with the time domain ordinary differential equations deduced in this study are presented in table 1. In general, it can be seen that the circuit presented in figure 1 as an electrical equivalent to a permanent magnet and the related expressions also can simulate the theoretical curves of the Stoner-Wohlfarth magnetic loops in very good fitting for most of the overlaps. The most distinct overlap was found for the SW3 curve (45°).

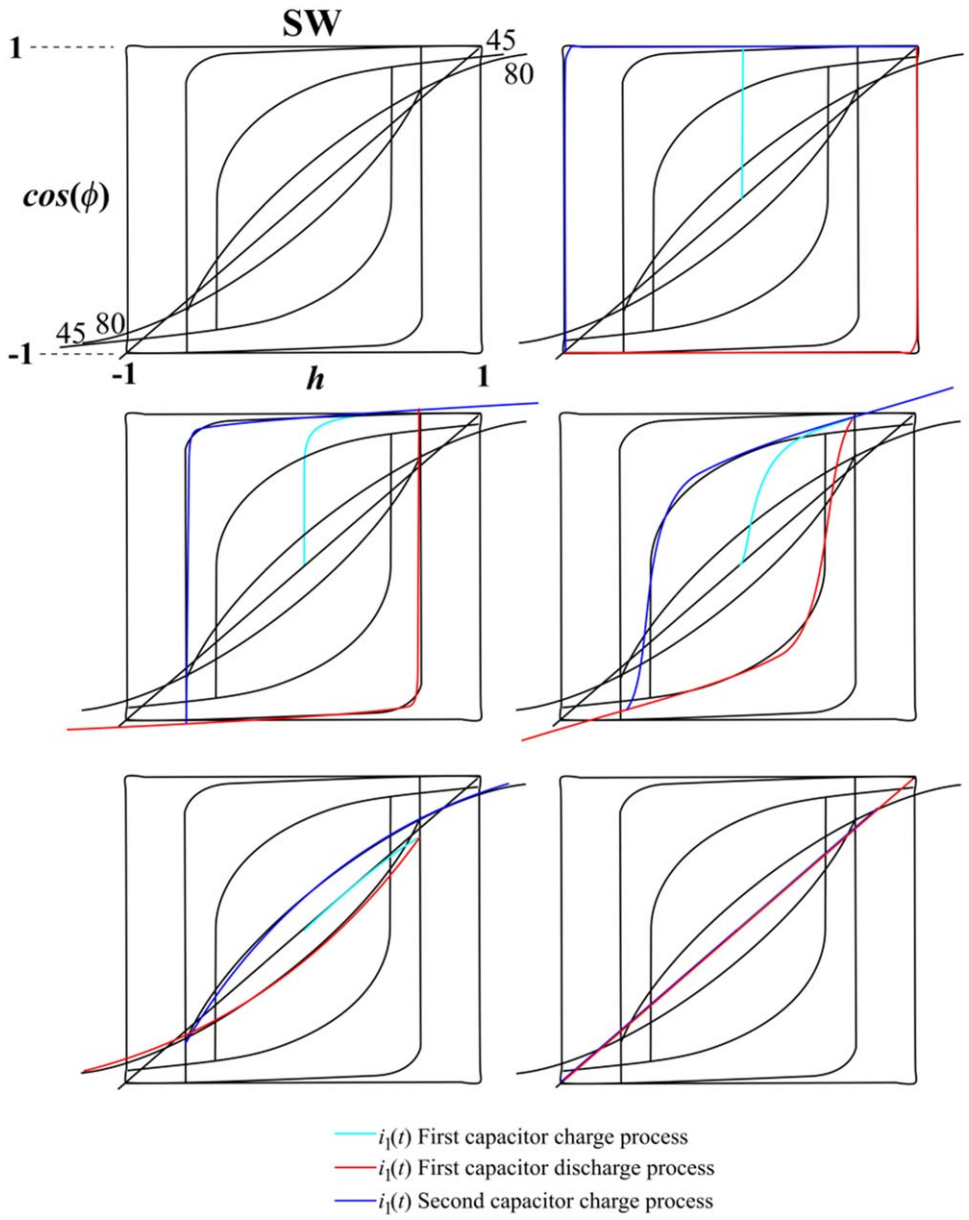

Figure 3. Graphical adaptation of the hysteresis loops for the Stoner-Wohlfarth (SW) model [22]. Curves are labeled according to the enclosed area (from SW1 for the first loop with the biggest area down to SW5 for the line at 45 degrees).

Table 1. Parameter values for the simulations curves shown in figure 3.

Name	Angle	R_1	R_2	C	L	β	$t_{(SC)}$
SW1	0	0.002	700	67	1×10^{-5}	0.015	67
SW2	10	0.015	12	65	1×10^{-5}	0.015	45
SW3	45	0.015	2.5	53	2.8×10^{-1}	0.015	40
SW4	80	0.83	5	89	1×10^{-4}	0.015	44
SW5	90	0.40	0.6	0.01	1×10^{-4}	0.015	67

4.2. Permanent magnets

The room temperature (298 K) demagnetization curve of a $Pr_{16}Fe_{76}B_8$ sintered magnet compared to a theoretical curve yielded by the deduced analytical equation (12) is shown in figure 4. The polarization or remanent magnetization with Tesla units has been used because this makes the X and *Y* axis with similar scales. Equivalent electric parameters for the magnet tested at room temperature (figure 4(a)) correspond to R_1

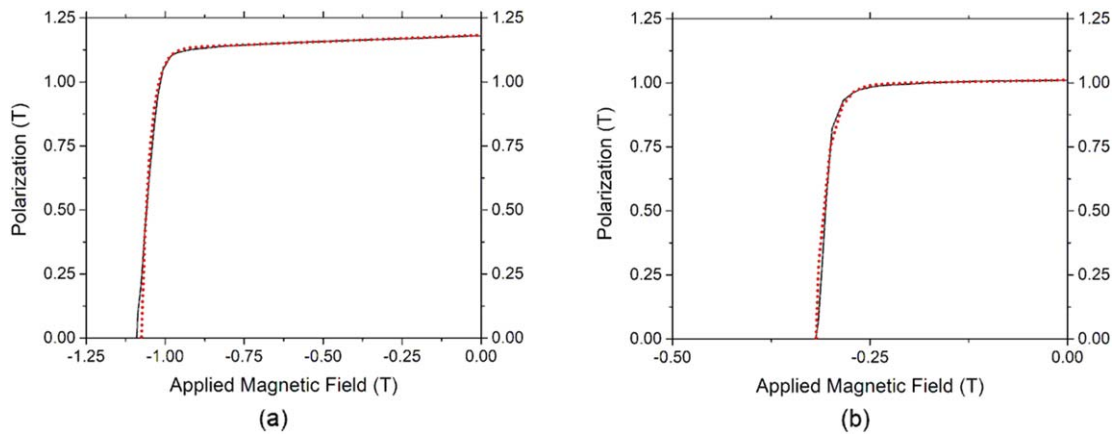

Figure 4. (a) Demagnetization curve of a $Pr_{16}Fe_{76}B_8$ sintered magnet (SF = 0.93) compared to a theoretical curve yielded by the analytical equation (red). (b) Demagnetization curve at 373 K of the $Pr_{16}Fe_{76}B_8$ sintered magnet (SF = 0.90) overlapped to the theoretical curve yielded by the analytical equation (red).

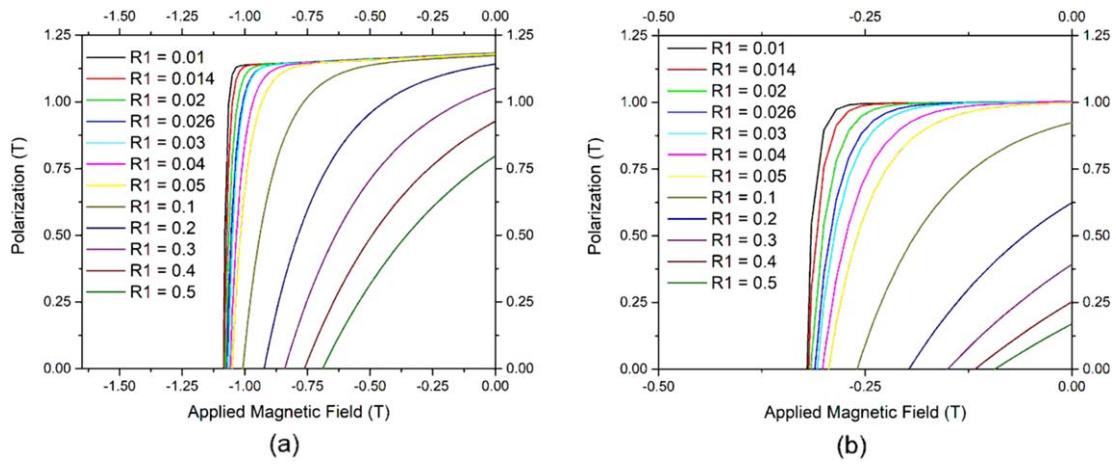

Figure 5. (a) Theoretical demagnetization curves for various values of R_1 with $R_2 = 22$; $C = 79$; $L = 1 \times 10^{-3}$; $\beta = 0.015$ and $t_{(SC)} = 73$. (b) Theoretical 373 K demagnetization curves for various values of R_1 with $R_2 = 30$; $C = 67$; $L = 1 \times 10^{-4}$; $\beta = 0.015$ and $t_{(SC)} = 22$.

$= 0.026$; $R_2 = 22$; $C = 79$; $L = 1 \times 10^{-3}$; $\beta = 0.015$ and $t_{(SC)} = 73$. An excellent overlap of the demagnetization curves has been obtained with these equivalent parameters. Equivalent electric parameters for this magnet tested at 373 K (figure 4(b)) correspond to $R_1 = 0.014$; $R_2 = 30$; $C = 67$; $L = 1 \times 10^{-4}$; $\beta = 0.015$ and $t_{(SC)} = 22$. Again, an excellent overlap of the demagnetization curves has been obtained with these new equivalent parameters.

The theoretical demagnetization curves for various values of R_1 with the other parameters kept constant are shown in figure 5. This parameter influences significantly the theoretical demagnetization curves of an equivalent permanent magnet. It affects the dramatically the shape of the curve (squareness factor), remanent polarization and intrinsic coercivity.

The theoretical demagnetization curves for various values of R_2 with the other parameters kept constant are shown in figure 6. This simulation parameter also influences significantly the theoretical demagnetization curves of an equivalent permanent magnet. It also affects the dramatically the shape of the curve but mainly the initial slope of the linear part of the curve, that is, the inclination, which can be related with the magnetic permeability of the permanent magnet. The polarization and intrinsic coercivity were also affected, but in a lesser extent than the previous case (R_1). It is also clear from figures 6(a) and (b) that the present model can model distinctly the effect of the temperature on the sintered permanent magnet since quite distinct curves have been obtained with both simulations. In other words, simulated curves for 373K on figure 6(b) are not a replica of the curves for room temperature shown in figure 6(a).

The theoretical demagnetization curves for various values of C with the other parameters kept constants are shown in figure 7. This parameter influences significantly the magnetic polarization of an equivalent permanent magnet. The intrinsic coercivity was also affected but in a lesser extent than the remanent polarization. As

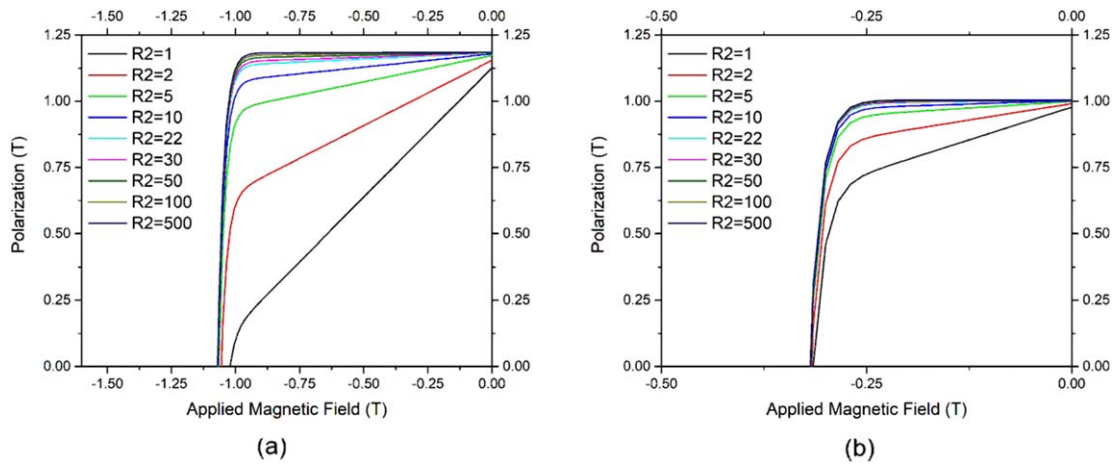

Figure 6. (a) Theoretical demagnetization curves for various values of R_2 with $R_1 = 0.026$; $C = 79$; $L = 1 \times 10^{-3}$; $\beta = 0.015$ and $t_{(SC)} = 73$. (b) Theoretical 373 K demagnetization curves for various values of R_2 with $R_1 = 0.014$; $C = 67$; $L = 1 \times 10^{-4}$; $\beta = 0.015$ and $t_{(SC)} = 22$.

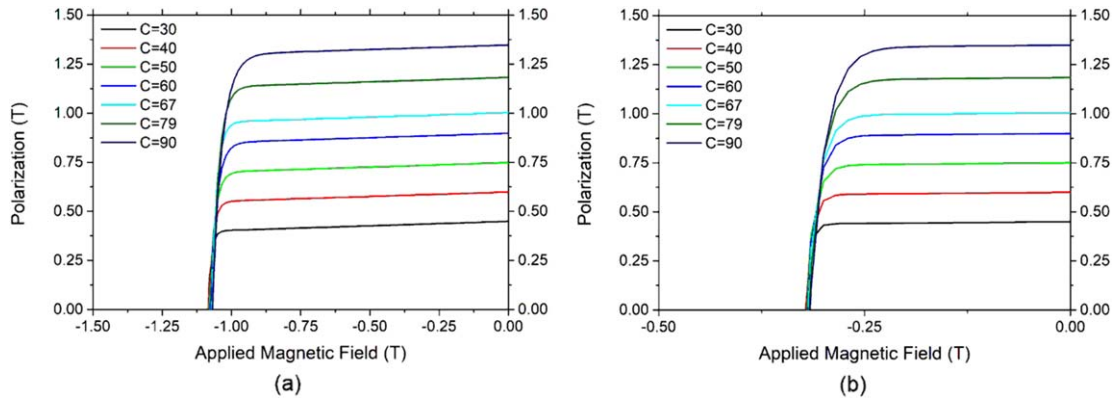

Figure 7. (a) Theoretical demagnetization curves for various values of C with $R_1 = 0.026$; $R_2 = 22$; $L = 1 \times 10^{-3}$; $\beta = 0.015$ and $t_{(SC)} = 73$. (b) Theoretical 373 K demagnetization curves for various values of C with $R_1 = 0.014$; $R_2 = 30$; $L = 1 \times 10^{-4}$; $\beta = 0.015$ and $t_{(SC)} = 22$.

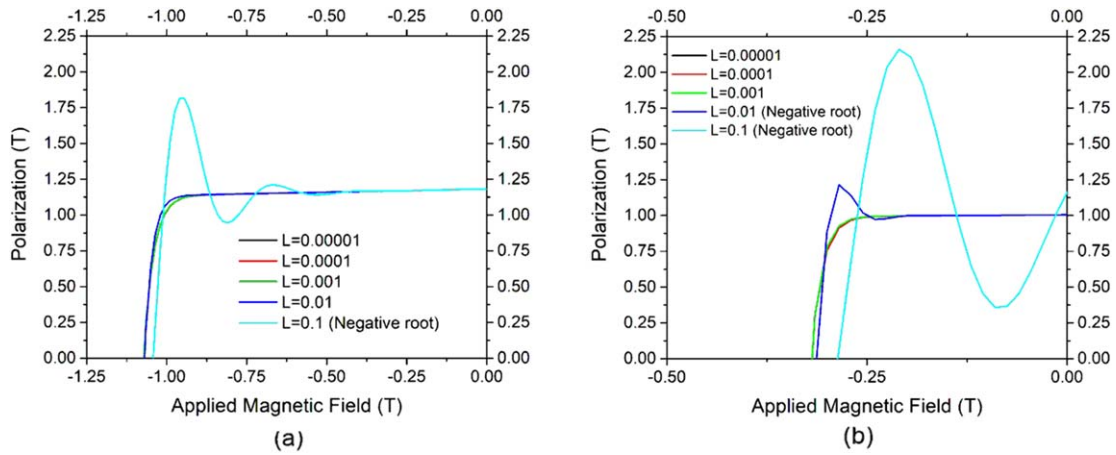

Figure 8. (a) Theoretical demagnetization curves for various values of L with $R_1 = 0.026$; $R_2 = 22$; $C = 79$; $\beta = 0.015$ and $t_{(SC)} = 73$. (b) Theoretical 373 K demagnetization curves for various values of L with $R_1 = 0.014$; $R_2 = 30$; $C = 67$; $\beta = 0.015$ and $t_{(SC)} = 22$.

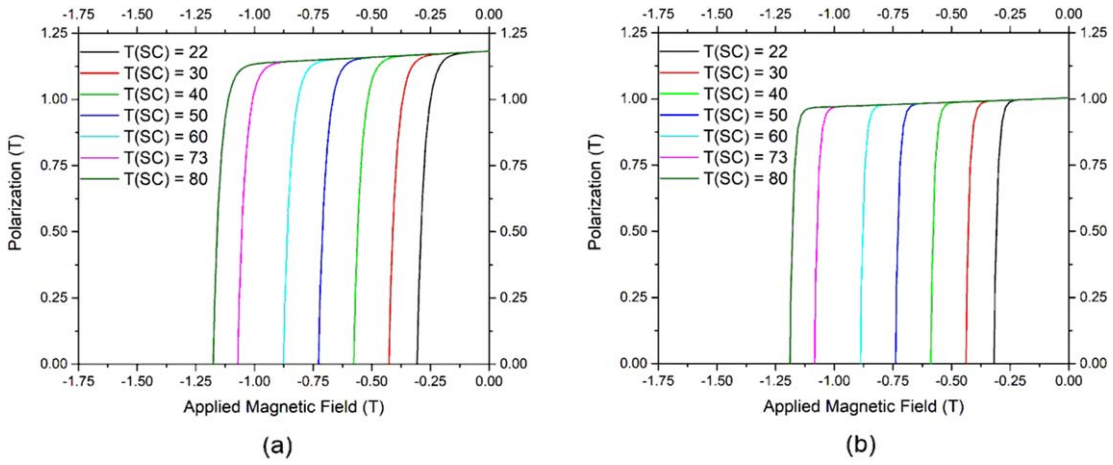

Figure 9. (a) Theoretical demagnetization curves for various values of $t_{(SC)}$ with $R_1 = 0.026$; $R_2 = 22$; $C = 80$; $L = 1 \times 10^{-3}$ and $\beta = 0.015$. (b) Theoretical 373 K demagnetization curves for various values of $t_{(SC)}$ with $R_1 = 0.014$; $R_2 = 30$; $C = 67$; $L = 1 \times 10^{-4}$ and $\beta = 0.015$.

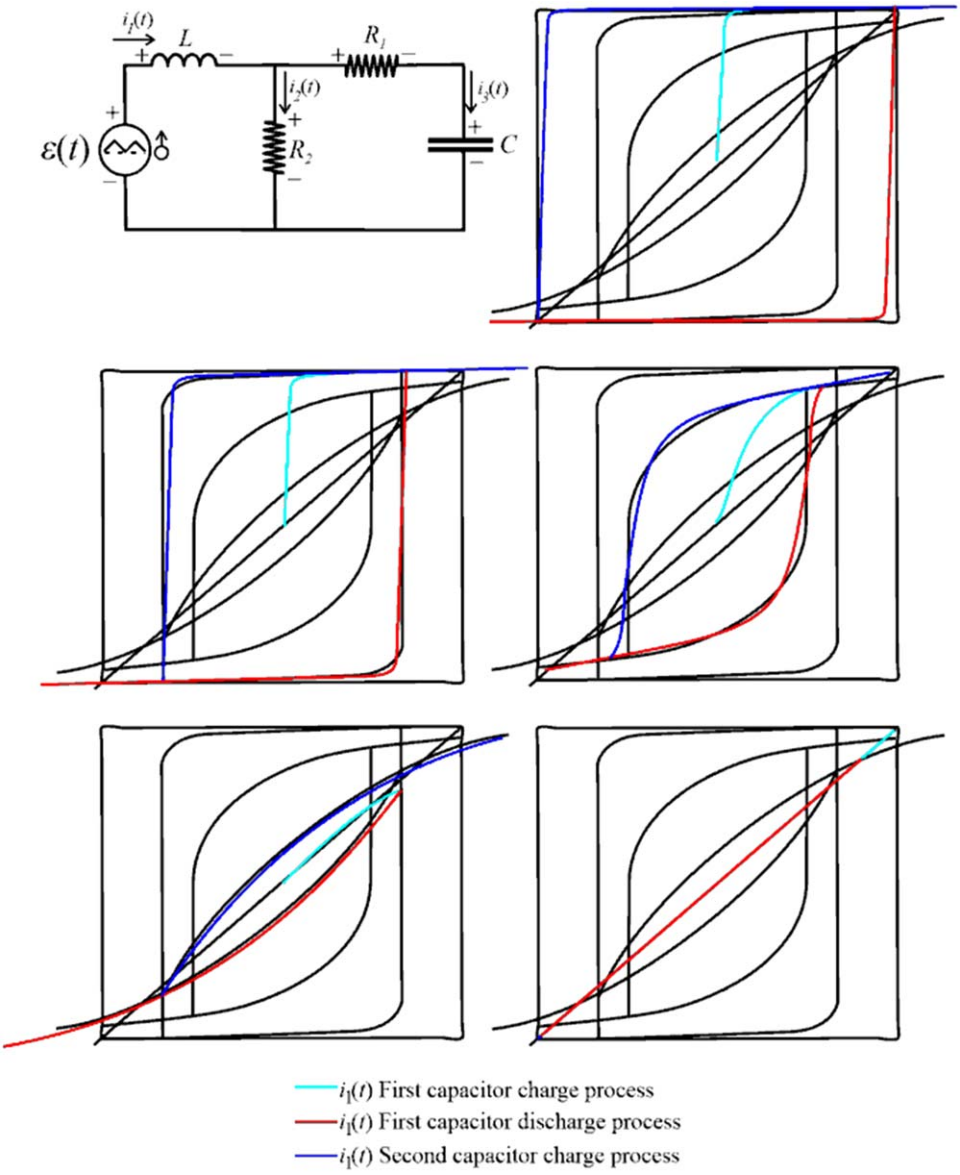

Figure 10. 2*RLC* circuit with R_1 in series with C and simulations curves for the SW model.

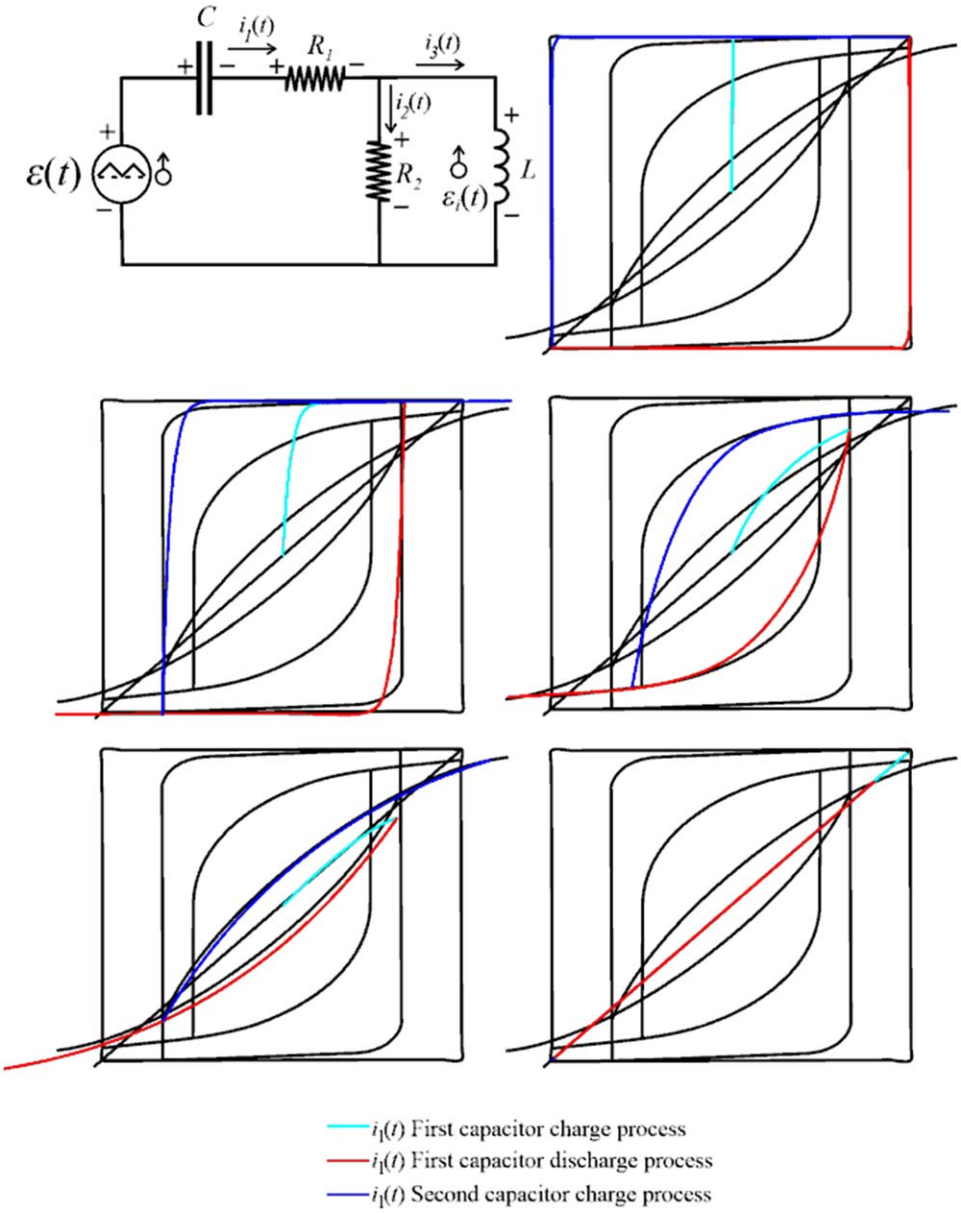

Figure 11. Theoretical simulation curve for the SW2, SW3, SW4 and SW5 for the analogous 2*RLC* circuit with R_1 in paralell with *C*.

observed in real rare earth permanent sintered magnets, with the reduction of remanence there is a tendency of improvement in the intrinsic coercivity [25]. The remanence of a sintered magnet is governed by several intrinsic and extrinsic parameters ($B_r = \langle \cos\Theta \rangle f P \mu_0 M_s$) [26]. Similarly, intrinsic coercivity is also a complex magnetic property dependent of several parameters ($\mu_0 H_c = \alpha \mu_0 H_A - N_{\text{eff}} J_s$, $\alpha = \alpha_\psi \alpha_K \alpha_{exc}$) [27–29]. Thus, it is possible to modify the curve to fit any experimental demagnetization curve but it is not possible to know which physical parameter is actually being changed on the remanence or coercivity.

The theoretical demagnetization curves for various values of *L* with the other parameters kept constants are shown in figure 8. Rather distinctly from the previous cases, this parameter influences only the squareness of the transition region between the horizontal and vertical linear lines of an equivalent permanent magnet. The intrinsic coercivities and remanences were not affected by changing this parameter. *L* value of 0.1 and 0.01 yield a negative root, which invalidates the theoretical equation for curve simulation. The theoretical demagnetization curves for various values of $t_{(SC)}$ with the other parameters kept constants are shown in figure 9. It can be readily noted that, similarly to room temperature simulations, these parameters also influence significantly the theoretical demagnetization curves of an equivalent permanent sintered rare earth magnet at 373 K.

4.3. Electric circuits

In order to verify if other electric circuits were also able to yield equations that simulate the demagnetization curve of permanent magnets various simpler circuits were also presented in this investigation. The good results

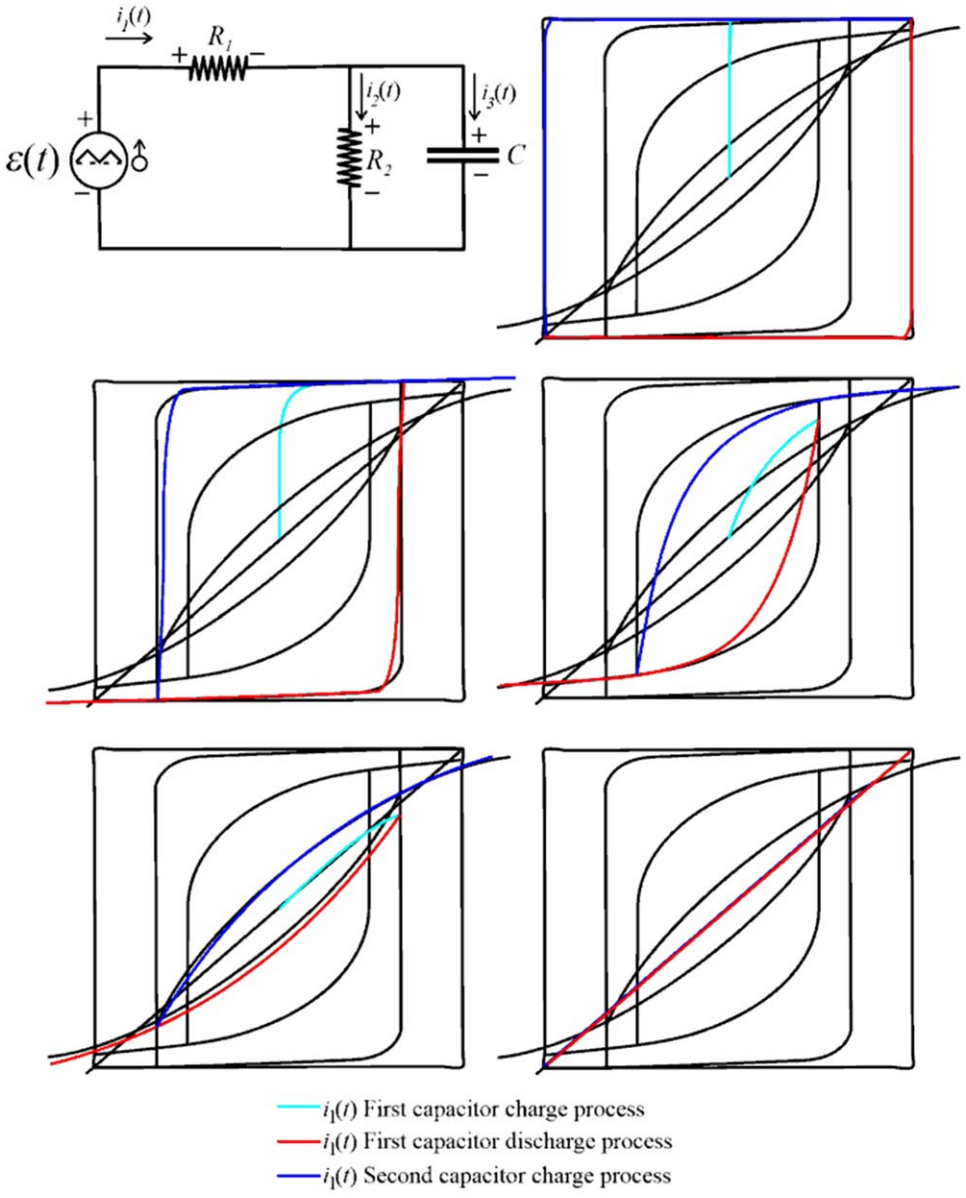

Figure 12. Theoretical simulation curve for the SW2, SW3, SW4 and SW5 for the analogous circuit 2*RC*.

presented previously can also be obtained using another 2*RLC* circuit, a variation in which the resistance R_1 is in series with the capacitance *C*, as shown in figure 10. It is also shown some simulation results of the SW curves based on this second analogous circuit. The SW simulation curves for this second circuit were similar to those obtained using of the 2*RLC* circuit that had the resistance R_1 in series with inductance *L*, shown in figures 1 and 2. The simulation graphs of the SW curves obtained with this second 2*RLC* electrical circuit were obtained with parameters different from those generated based on the first 2*RLC* analogous circuit for the simple constructive matter (the equations of the first one were different, but obtained in the same way). In this work it was preferred to use the 2*RLC* circuit with R_1 in series with the inductance for a simple matter of choice and nothing else.

A third electrical analogy circuit used for modeling and simulations together with SW1 is depicted in figure 11. This analogy circuit does not allow changing the horizontal inclination of the curves, presenting poorer simulations loops than the previously shown circuits. A fourth electrical analogy circuit used for modeling and simulations together with SW1 is depicted in figure 12. The equations for this analogy circuit allows better simulations loops than the previously one, and would be quite similar to the 2*RLC* circuit. This is rather expected given the small values (very closed to zero) employed for *L* in the 2*RLC* circuits.

A fifth electrical analogy circuit (*RC*) used for modeling and simulations together with SW1 is depicted in figure 13. This analogy circuit also does not allow changing the horizontal inclination of the curves, presenting poorer simulations loops than the previously shown circuits. Figure 14 shows various circuits that do not allow simulating the Stoner-Wohlfarth loops. It should be noted that the input inductance *L* can be eliminated for

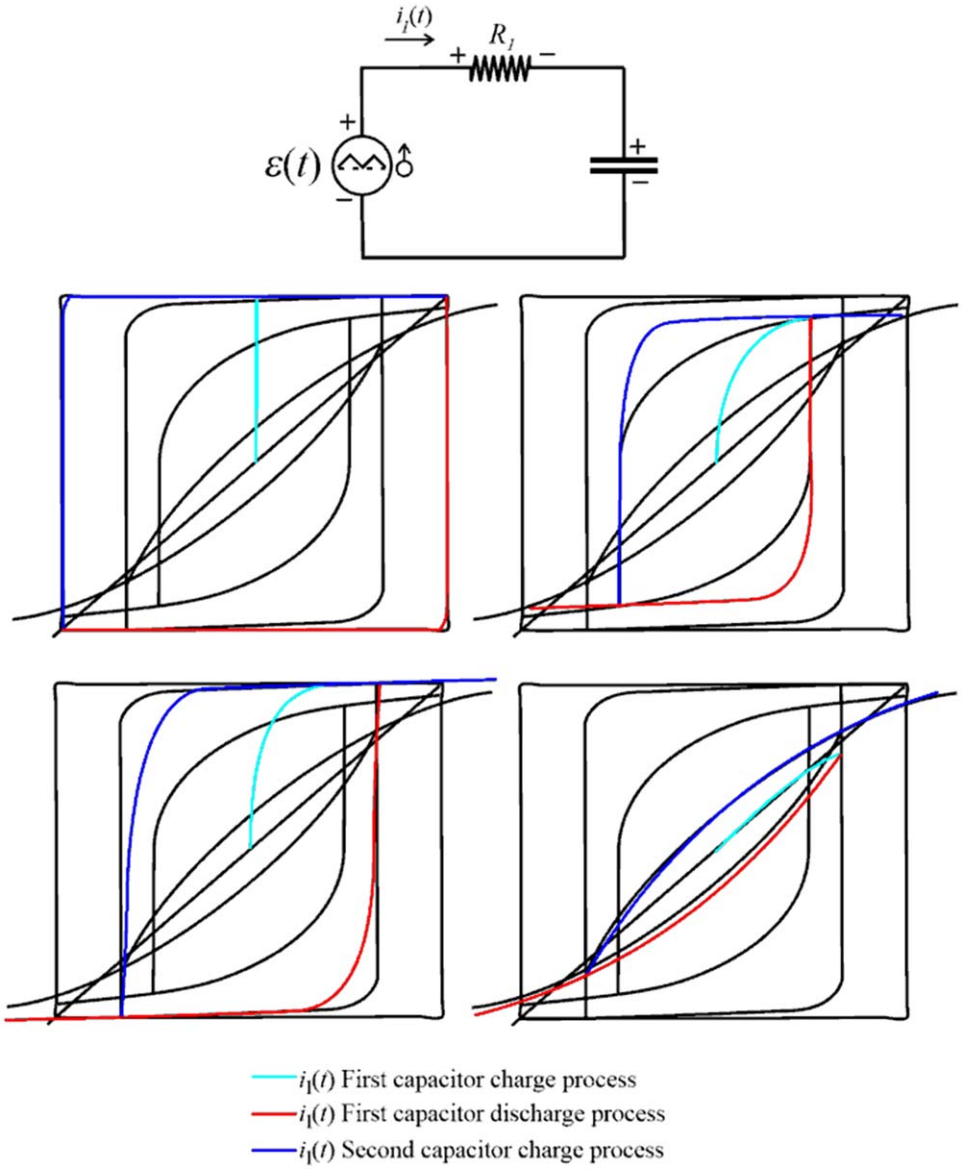

Figure 13. Theoretical simulation curve for the analogous circuit *RC*.

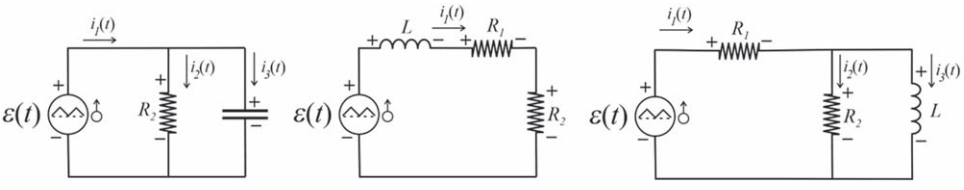

Figure 14. Theoretical circuits that yield equations that do not allow SW loops simulations.

simulations that include only the second quadrant, however, it is necessary for the simulation of hysteresis curves of the first and third quadrants for some types of magnets. Figure 15(a) shows the demagnetization curve of a $Pr_{16}Fe_{76}B_8$ sintered magnet compared to a theoretical curve produced by an analytical equation based on a *RC* series circuit and (b) at 373 K. Somewhat better fitting overlap was obtained in the latter.

At this juncture, the physical meaning of these electrical parameters can only be inferred based on the microstructural knowledge of the permanent magnet. Nevertheless, some imperfections on the magnet of practical nature can be attributed to the resistances on the electrical circuit. A magnet has pores, secondary phases and lattice defects, which could be represented by these resistances. R_1 can be attributed to

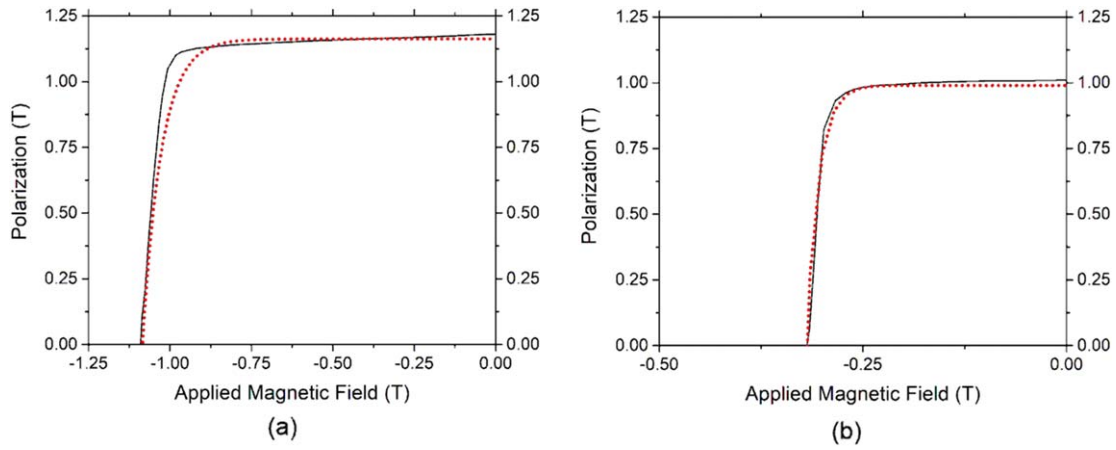

Figure 15. (a) Demagnetization curve of a $Pr_{16}Fe_{76}B_8$ sintered magnet (SF = 0.93) compared to a theoretical curve produced by an analytical equation based on a *RC* series circuit ploted in (red) with $R_1 = 0.05$; $C = 77{,}5$; $\beta = 0.015$ and $t_{(SC)} = 75$. (b) Demagnetization curve at 373 K of the $Pr_{16}Fe_{76}B_8$ sintered magnet (SF = 0.90) compared to a theoretical curve produced by an analytical equation based on a *RC* series circuit plotted in (red) with $R_1 = 0.015$; $C = 66$; $\beta = 0.015$ and $t_{(SC)} = 22$.

microstructural features since it changes M_r and ${}_iH_c$. Similarly, R_2 can also be microstructural once for the 373K curve only ${}_iH_c$ is influenced. C is mainly related to the saturation polarization once M_r is the main changed parameter. The model does not allow simulating magnets containing magnetically soft secondary phases that yield kinks on the second quadrant of the demagnetization curve. The alloy composition, additions and processing conditions can be changed and the resulting magnetic properties can be associated to these electrical parameters in order to obtain a better understanding of the physical meaning of this equivalent electrical model. Further investigations are underway in an attempt to associate magnetic behavior to the electrical simulations parameters.

Intuitively one might think that a real permanent magnet could be exchanged by a coil with an inductance L as it is carried out in most practical applications. This seems not to be the case as far as the material is concerned, as show in figure 14 for circuits that do not allow simulations of the SW curves. As far as the capacitor to work very well in the magnet analogous it must be remembered that very often in the literature a magnet is depicted as a charged capacitor with the positive and negative charges in the north and south pole, respectively. Although the present time domain equations model using a 2*RLC* circuit does not allow the simulations of non-fully magnetized permanent magnets it still presents more flexibility than previous attempts reported in the literature [30, 31]. The previous model presented in the literature showed that the error function equation was used because the authors were interested in the cumulative probability that the grains have reversed to the left of the remanence. The first part of the equation was the dominant term of the equation in the second quadrant. The second term of this equation captures the adjustment for alignment and is a smaller correction. Its effect was easier to see in the first quadrant, with a slight positive slope, where the probability term is constant, fixed at 1 [30]. Apart from this equation model using the error function equation no other simulations models have been reported in the literature for M x H demagnetization curves.

The potential application of the proposed approach has impact on the design and optimization of permanent magnets for specific industrial and scientific applications. Thus, by systematically varying only the $\langle \cos \Theta \rangle$ of various sintered magnets it is possible to verify which electrical parameters are necessary to be altered as well, which would lead to better prediction of practical magnets behavior.

5. Conclusions

It has been shown that it is possible to simulate the demagnetization curves of permanent sintered magnets using time domain analytical expressions obtained using an electric equivalent circuit analogous to a closed magnetic circuit. The present model uses only a triangular electrical potential source, a capacitor, an inductor and two resistances. Each individual equivalent electric parameter influences a specific region of the demagnetization curve of the permanent magnet, which is associated to a physical characteristic of the magnetic alloy and to the processing conditions. As far as the simulations curves are concerned, the 2*RLC* circuit works very satisfactorily in most cases whereas other possible circuits have some kind of hindrances for some simulations curves. It is possible to simulate the demagnetization curve of rare earth magnets and also any other types of permanent

magnets. Although the model allows simulating any demagnetization curve it does not discriminate which physical parameter is being changed on the permanent magnet.

Acknowledgments

The work of A P R Fernandez was supported by the FACULTY SENAI SÃO PAULO - Campus Theobaldo De Nigris - Mooca, São Paulo, Brazil. This work was supported by INCT-PATRIA: FAPESP - 14/50887-4; CAPES - 23038.000776/2017-54 ; CNPq - 465719/2014-7).

Data availability statement

All data that support the findings of this study are included within the article (and any supplementary files).

Declaration of competing interest

The authors declare that there is no conflict of interest.

Data access statement

The data that support this research and the step-by-step obtaining of the equations presented in it can be obtained directly from Dr Antonio Paulo Rodrigues Fernandez via email aprfff@alumni.usp.br.

Ethics statement

This research did not perform studies on people or animals.

ORCID iDs

Antonio Paulo Rodrigues Fernandez https://orcid.org/0000-0003-2692-6074
Rubens Nunes de Faria Junior https://orcid.org/0000-0003-0975-0863

References

[1] Gross B 1956 Electrical analogs for viscoelastic systems *J. Polym. Sci.* **20** 371–80
[2] Ala G, Paola M D, Francomano E, Li Y and Pinnola F P 2014 Electrical analogous in viscoelasticity *Com. Nonlinear Sci Numer Simulat.* **19** 2513–27
[3] Greene P R and Medved V 2017 Electrical analogs for Kelvin & Maxwell viscoelastic materials: applications to cornea & sclera *New Front Ophthalmol* **3** 1–4
[4] Kucera O 2010 Electrical analogy to an atomic force microscope *Radioengineering* **19** 168 (https://radioeng.cz/fulltexts/2010/10_01_168_171.pdf)
[5] Beck P A and Oliveira C 2021 RLC circuit: analogy with mechanical systems *Proceeding Series of the Brazilian Society of Computational and Applied Mathematics, V.* **8** 1 (https://academia.edu/76417627/Proceeding_Series_of_the_Brazilian_Society_of_Computational_and_Applied_Mathematics)
[6] Save Y D, Narayanan H and Patkar S B 2011 Solution of partial differential equations by electrical analogy *Journal of Computational Science* **2** 18–30
[7] Meeker D 2009 Mechanical and electrostatic analogies to permanent magnets Analogies:Finite Element Method Magnetics (femm. info). (https://femm.info/wiki/Analogies)
[8] Chavanne J, Chubar O, Elleaume P and Vaerenbergh P V Nonlinear numerical simulation of permanent magnets *Proc. of European Particle Accelerator Conf., EPAC 2000, Vienna, Austria* 2316–8 (https://accelconf.web.cern.ch/e00/PAPERS/WEP4B03.pdf)
[9] Pyrhönen J, Ruoho S, Nerg J, Paju M, Tuominen S, Kankaanpää H, Stern R, Boglietti A and Uzhegov N 2014 Hysteresis losses in sintered NdFeB permanent magnets in rotating electrical machines *IEEE Trans. Ind. Electron.* **62** 857–65 (https://ieeexplore.ieee.org/stamp/stamp.jsp?tp=&arnumber=6891224)
[10] Jubband G A and McCurrie R A 1987 Hysteresis and magnetic viscosity in a Nd-Fe-B permanent magnet *IEEE transactions on magnetics, V23* **2** 1801–5 (https://ieeexplore.ieee.org/stamp/stamp.jsp?arnumber=1065064)
[11] Fliegans J , 2019 Coercivity of NdFeB-based sintered permanent magnets: experimental and numerical approaches *Doctoral Dissertation, Université Grenoble Alpes* 64–9 (https://tel.archives-ouvertes.fr/tel-02635105/)
[12] Rizinia Company News 2020 Demagnetization curve squareness Q and knee point Hk (https://rizinia.com/demagnetization-curve-squareness-q-and-knee-point-hk.html)
[13] Niedra J M and Overton E 1991 23 to 300 °C demagnetization resistance of samarium-cobalt permanent magnets *NASA Technical paper* **3119** 1–8 (https://ntrs.nasa.gov/api/citations/19920002034/downloads/19920002034.pdf)

[14] Hayerikhiyavi M and Dimitrovski A 2021 Improved gyrator-capacitor modeling of magnetic circuits with inclusion of magnetic hysteresis, university of central florida, MPRA paper No. 109495, posted 31 Aug 2021 15:27 UTC, Online at (https://mpra.ub.uni-muenchen.de/109495/)
[15] Hamill D C 1994 Gyrator-capacitor modeling: a better way of understanding magnetic components *Proceedings of 1994 IEEE Applied Power Electronics Conference and Exposition - ASPEC⇗94, Orlando, FL, USA* **1** 326–32 (https://ieeexplore.ieee.org/stamp/stamp.jsp?arnumber=316381)
[16] Lee Y S and Chow M H L , 2007 Modelling and teaching of magnetic circuits *Asian Power Electronics Journal* **1** 15–20 (http://perc.polyu.edu.hk/APEJ/APEJ/Volume1/paper02.pdf)
[17] Hamilton N C 2016 Ferrites: magnetic and electric equivalent circuits and the complex permeability spectra *Conferences : active and Passive RF Devices Seminar* **17-17** 1–8 (https://ieeexplore.ieee.org/stamp/stamp.jsp?tp=&arnumber=7479388)
[18] Sahdev S K 2017 *Electrical Machines* (Cambridge University Press) 1st Edition5–6 (https://referenceglobe.com/CollegeLibrary/library_books/20200125041045198204Electrical%20Machines%20by%20Mr.%20S.%20K.%20Sahdev.pdf)
[19] González G G and Ehsani M 2018 Power-Invariant magnetic system modeling *Int. J. Magnetics Electromag* **4** 012 (https://vibgyorpublishers.org/content/ijme/fulltext.php?aid=ijme-4-012)
[20] Takahashi S, Ogasawara S and Novel A 2020 Simulation model for common-mode inductors based on permeance-capacitance analogy *2020 IEEE Energy Conversion Congress and Exposition* **11-15** 5862–9 (https://ieeexplore.ieee.org/abstract/document/9235976)
[21] Fernandez A P R, Perigo E A and Faria R N 2021 Analytical expressions for electrochemical supercapacitor with potential dependent capacitance *Journal of Energy Storage* **43** 103156
[22] Stoner E C and Wohlfarth E P 1948 A mechanism of magnetic hysteresis in heterogeneous alloys *Philosophical Transactions of the Royal Society A, Mathematical and Physical Sciences* **204** 599–642
[23] Soares E P, Périgo E A, Takiishi H, Motta C C and Faria R N 2005 A study of PrFeB magnets produced by a low-cost powder method and the hydrogen decrepitation process *Mater. Res.* **8** 143–5 (https://scielo.br/j/Mr/a/kTyW6fMrBRwLrCSCSfHvvhC/?lang=en)
[24] Ma B M and Narasimhan K S V L 1986 Temperature dependence of magnetic properties of Nd-Fe-B *magnets, J. Magn. Magn. Mater.* **54–47** 559–62 (https://sciencedirect.com/science/article/pii/0167577X85900874)
[25] Faria R N 2002 The influence of zirconium addition and process parameters on the magnetic properties of Pr-Fe-B sintered magnets *J. Magn. Magn. Mater.* **238** 56–64 (https://sciencedirect.com/science/article/pii/S0304885301007016)
[26] Faria R N, Castro A R M and Lima N B , 2002 Relation between grain alignment and magnetic properties of Pr-Fe-B sintered magnets *J. Magn. Magn. Mater.* **238** 38–46 (https://sciencedirect.com/science/article/pii/S0304885301007053)
[27] Kronmüller H and Fähnle M 2003 *Micromagnetism and the Microstructure of Ferromagnetic Solids* (Cambridge Univ. Press) (https://books.google.com.br/books/about/Micromagnetism_and_the_Microstructure_of.html?id=h6nKtwcYyNEC&redir_esc=y)
[28] Li J 2016 Investigation of the resistance to demagnetization in bulk rare-earth magnets comprised of crystallographically-aligned, single-domain crystallites with modified intergranular phase *PhD dissertation, Dept. Phys* (MichiganTechnol. Univ.) (https://digitalcommons.mtu.edu/etdr/131/)
[29] Périgo E A and Faria R N 2020 Experimental assessment of coercivity microstructural parameters of a Nd-Fe-B sintered magnet *in IEEE Magnetics Letters* **11** 1–57505705
[30] Trout S Estimating complete hysteresis loops of permanent magnets using excel Publication at (https://researchgate.net/publication/351037336_Estimating_Complete_Hysteresis_Loops_of_Permanent_Magnets_Using_Excel)
[31] Parker R J 1958 Understanding and predicting permanent magnet performance by electrical analog methods *J. Appl. Phys.* **29** 409